Fundamental Indirect Noise Generation by Interactions between Entropy, Vorticity and Acoustic Waves in the Context of Aero Engine Applications

Wolfram Christoph ULLRICH[1]; Moritz SCHULZE[1]; Thomas SATTELMAYER[1]

[1] Technische Universität München, Germany

ABSTRACT

In aero engines indirect noise is released by the acceleration of entropy and vorticity waves in the turbine, which are in turn created mainly further upstream in the combustor by unsteady combustion. Recent studies show that these interactions contribute substantially to the total emitted core noise. Consequently a detailed knowledge of the sources of entropy and vorticity waves and their interactions with mean flow and acoustics is essential for the efficient development of technologies to reduce indirect noise. In this study, a generic convergent-divergent nozzle configuration is considered as a simplified model of the transonic turbine vane flow to study entropy noise as well as the acoustic scattering behavior. A two step numerical approach is applied consisting of RANS mean flow simulations and succeeding acoustic simulations in frequency domain based on linearized Navier-Stokes equations. Source terms for both waves are deduced from linearized entropy and vorticity equation and evaluated spatially. Important interactions between entropy, vorticity and acoustic waves and the mean flow are highlighted and confirmed by an energy analysis. This analysis can be applied to real aero engine combustors and turbines and enables to quickly identify the impact of the different source mechanisms on indirect noise.

Keywords: Indirect noise, entropy, vorticity   I-INCE Classification of Subjects Number(s): 21.1

1.   INTRODUCTION

The development of efficient technologies to reduce aero engine noise is essential to meet the requirements of the future air traffic. For instance, jet noise has been successfully reduced by increasing the engine bypass ratio and the invention of chevron nozzles. But as the exhaust nozzle exit velocity decreases, the noise associated with the combustion, termed core noise, becomes the dominant effect which has already been reported by Cumpsty (1, 2). The combustion noise originates from two different mechanisms, more specifically the direct and indirect noise. Direct noise is generated by unsteady combustion leading to pressure and temperature fluctuations. These temperature inhomogeneities or entropy waves are convected downstream into the turbine where they release additional sound, the indirect noise, due to the acceleration in the mean flow. Recent analytical studies by Leyko et al. (3) and Duran and Moreau (4) have shown that the indirect noise phenomenon significantly contributes to the overall core noise. Analytical models by Howe (5) and experiments by Kings (6, 7) have shown that indirect noise is also produced by accelerated vorticity waves. Overall, this explains why a detailed analysis and better understanding of the sources and interactions of entropy and vorticity waves is necessary to develop efficient technologies to reduce indirect noise in advance at its source.

In this study a convergent-divergent nozzle configuration, known as the Entropy-Wave Generator (EWG) by Bake et al. (8), is examined as the most abstract model of a turbine vane flow where significant interactions between acoustic, entropy and vorticity waves occur. In the experiment entropy waves are excited by heating wires located in an upstream duct. Several microphones are installed to measure the acoustic pressure response in the downstream duct for subsonic and transonic flow conditions. The EWG was object of several analytical studies by Leyko et al. (9), Howe (5) or Duran and Moreau (4) who all together have proven the indirect noise

---

[1] ullrich@td.mw.tum.de,Ph.D.candidate

[2] schulze@td.mw.tum.de,Ph.D.candidate

[3] sattelmayer@td.mw.tum.de,ProfessorPh.D.

generation theoretically. Moreover, the noise spectra were accurately reproduced by means of Large-Eddy simulations (LES), performed by Leyko et al. (9), as well as URANS and Linearized Euler equations (LEEs) based simulations by Bake et al. (8). To our knowledge, a source term evaluation was only performed by Bake et al. (8) which is based on the extended wave equation for reacting flows as derived by Dowling (10) and the energy balance by Morfey (11) and Myers (12). A detailed analysis of the source and interaction mechanisms of entropy and vorticity waves which finally leads to the indirect noise has not been done yet.

In order to determine these complex interaction mechanisms in the EWG a two step hybrid approach is applied which was initially implemented by Gikadi (13) and validated for several test cases with increasing complexity (14, 15). In a first step the nozzle mean flow is computed by a stationary RANS simulation in time space, which serves as a linearization point for the superposition of small acoustic, entropy and vortical fluctuations. The propagation of these fluctuations in presence of the mean flow is described by the linearized Navier-Stokes equations (LNSEs) which are solved in frequency space in a succeeding step by stabilized finite element discretization. By this means, Ullrich et al. (16) successfully computed the acoustic response to the entropy excitation and validated it by experimental measurements. Additionally, the acoustic scattering behavior of the nozzle was determined by the two source-location method and compared to analytical models and simple numerical solutions. In the present study, the different interaction mechanisms are deduced from linearized energy and vorticity equation, discussed extensively and evaluated spatially. A first order energy analysis is applied on the EWG which confirms the results. The analysis presented can be applied to real aero engine combustors to account for different interaction mechanisms already during the aerothermodynamic design stage. In comparison to URANS or LES simulations, instationary simulations do not have to be carried out in frequency domain. Another advantage is that the identification of coherent structures like entropy and vorticity waves requires no complex post-processing steps such as dynamic mode decomposition (DMD) (17) or proper orthogonal decomposition (POD). Overall, this leads to a remarkable reduction of computational effort.

2.   GOVERNING EQUATIONS

The analysis is based on the linear assumption so that an arbitrary flow quantity ϕ is described by small fluctuations $(\cdots')$ around its mean time averaged state $(\bar{\cdots})$, i.e.

$$\phi(\boldsymbol{x},t) = \bar{\phi}(\boldsymbol{x}) + \phi'(\boldsymbol{x},t), \tag{1}$$

with $\boldsymbol{x}$ being the position vector and t the time. The linearized Navier-Stokes equations are obtained by the substitution of the separation-approach (1) into the Navier-Stokes equations in conjunction with the neglection of higher order terms. The mean flow state is subtracted from the linearized equations in order to separate the fluctuating quantities from the mean field. The fluctuations are assumed to be harmonic in time so that any quantity is expressed in terms of its complex amplitude $\hat{\phi}$ and complex exponential function

$$\phi'(\boldsymbol{x},t) = \mathrm{Re}\{\hat{\phi}(\boldsymbol{x})\,e^{\mathrm{i}\omega t}\}. \tag{2}$$

This procedure finally yields the frequency-transformed linearized Navier-Stokes equations (LNSEs) with the circular frequency $\omega = 2\pi f$ as parameter

$$\mathrm{i}\omega\hat{\rho} + \bar{\boldsymbol{u}}\nabla\hat{\rho} + \hat{\boldsymbol{u}}\nabla\bar{\rho} + \bar{\rho}\nabla\cdot\hat{\boldsymbol{u}} + \hat{\rho}\nabla\cdot\bar{\boldsymbol{u}} = 0, \tag{3}$$

$$\mathrm{i}\omega\bar{\rho}\hat{\boldsymbol{u}} + \bar{\rho}\bar{\boldsymbol{u}}\nabla\hat{\boldsymbol{u}} + \bar{\rho}\hat{\boldsymbol{u}}\nabla\bar{\boldsymbol{u}} + \hat{\rho}\bar{\boldsymbol{u}}\nabla\bar{\boldsymbol{u}} + \nabla\hat{p} - \eta\left[\Delta\hat{\boldsymbol{u}} + \frac{1}{3}\nabla\left(\nabla\cdot\hat{\boldsymbol{u}}\right)\right] - \bar{\rho}\hat{\boldsymbol{f}} - \hat{\rho}\bar{\boldsymbol{f}} = \boldsymbol{0}, \tag{4}$$

$$\mathrm{i}\omega\hat{p} + \bar{\boldsymbol{u}}\nabla\hat{p} + \hat{\boldsymbol{u}}\nabla\bar{p} + \kappa\bar{p}\nabla\cdot\hat{\boldsymbol{u}} + \kappa\hat{p}\nabla\cdot\bar{\boldsymbol{u}} - (\kappa-1)\left\{2\eta\left[\nabla\bar{\boldsymbol{u}}:\nabla\hat{\boldsymbol{u}} + \nabla\bar{\boldsymbol{u}}:\nabla\hat{\boldsymbol{u}}^T - \frac{2}{3}\left(\nabla\cdot\bar{\boldsymbol{u}}\right)\left(\nabla\cdot\hat{\boldsymbol{u}}\right)\right] + \lambda\Delta\hat{T} + \hat{q}_V\right\} = 0. \tag{5}$$

This set of five linear partial differential equations is solved for the unknown fluctuating density $\hat{\rho}$, velocities $\hat{\boldsymbol{u}}$ and pressure $\hat{p}$ while the corresponding mean flow quantities $\bar{\rho}, \bar{\boldsymbol{u}}$ and $\bar{p}$ are given from RANS simulation. Viscous and thermal diffusion in the calorically perfect gas are characterized by its dynamic viscosity η and thermal conductivity λ. $\hat{\boldsymbol{f}}$ terms body forces and $\hat{q}_V$ the fluctuating heat release. Temperature $\hat{T}$ and entropy fluctuations $\hat{s}$ are closely related to each other and can be recovered from the $(\hat{\rho}, \hat{\boldsymbol{u}}, \hat{p})$-formulation by means of linearized equation of state

$$\hat{T} = \bar{T}\left(\frac{\hat{p}}{\bar{p}} - \frac{\hat{\rho}}{\bar{\rho}}\right), \qquad\qquad \hat{s} = c_v\frac{\hat{p}}{\bar{p}} - c_p\frac{\hat{\rho}}{\bar{\rho}}, \tag{6}$$

where the isobaric and isochoric heat capacities are represented by c_p and c_v, respectively. Kovasznay (18) and Chu (19) have demonstrated that the LNSEs feature three different linear transport processes of acoustic, entropy and vortical disturbances $\hat{\boldsymbol{\Omega}} = \nabla \times \hat{\boldsymbol{u}}$. Unlike acoustic waves, which propagate at speed of sound $\bar{c}$ in the relative frame of the mean flow, entropy and vorticity waves are convected with mean flow. Sources of entropy waves can be identified by rewriting the linearized energy Eq. (5) in terms of entropy giving

$$\bar{\rho}\bar{T}\left(i\omega\hat{s} + \bar{\boldsymbol{u}}\nabla\hat{s}\right) = -\left(\underbrace{\hat{\boldsymbol{u}}\bar{\rho}\bar{T}}_{I} + \underbrace{\bar{\boldsymbol{u}}\hat{\rho}\bar{T}}_{II} + \underbrace{\bar{\boldsymbol{u}}\bar{\rho}\hat{T}}_{III}\right)\nabla\bar{s} + \underbrace{2\eta\left[\nabla\bar{\boldsymbol{u}}:\nabla\hat{\boldsymbol{u}} + \nabla\bar{\boldsymbol{u}}:\nabla\hat{\boldsymbol{u}}^T - \frac{2}{3}\left(\nabla\cdot\bar{\boldsymbol{u}}\right)\left(\nabla\cdot\hat{\boldsymbol{u}}\right)\right]}_{IV} + \underbrace{\lambda\Delta\hat{T}}_{V} + \underbrace{\hat{q}_V}_{VI}.$$
(7)

The left hand side of Eq. (7) is the frequency-transformed material derivative of the entropy $\mathrm{D}s'/\mathrm{D}t = \partial s'/\partial t + \bar{\boldsymbol{u}}\nabla s'$. As a consequence, all terms on the right hand side represent sources or sinks of entropy waves as they travel along their stream-path. Entropy waves are influenced by or arise from

- interactions of acoustics, vorticity (reaction terms I and II) and entropy (reaction term III) with non-homentropic mean flow,
- dissipation of acoustics and vorticity into entropy (source term IV) described by linearized dissipation function,
- diffusion and dissipation of themselves due to heat conduction (elliptical term V), and
- fluctuating heat sources (term VI).

The mean flow is called homentropic if it is isentropic ($\mathrm{D}\bar{s}/\mathrm{D}t = 0$) and its entropy is constant ($\nabla\bar{s} = 0$). Therefore, regions with strong mean entropy gradients such as flames, mixing shear layers or shocks are examples for non-homentropic conditions. The propagation of vorticity waves is described by the linearized vorticity equation which is naturally incorporated in the momentum Eq. (4) and can be derived by taking its curl, as described for instance by Lieuwen (20)

$$i\omega\hat{\boldsymbol{\Omega}} + \bar{\boldsymbol{u}}\nabla\hat{\boldsymbol{\Omega}} = -\underbrace{\hat{\boldsymbol{u}}\nabla\bar{\boldsymbol{\Omega}}}_{I} + \underbrace{\bar{\boldsymbol{\Omega}}\nabla\hat{\boldsymbol{u}}}_{II} + \underbrace{\hat{\boldsymbol{\Omega}}\nabla\bar{\boldsymbol{u}}}_{III} - \underbrace{\bar{\boldsymbol{\Omega}}\nabla\cdot\hat{\boldsymbol{u}}}_{IV} - \underbrace{\hat{\boldsymbol{\Omega}}\nabla\cdot\bar{\boldsymbol{u}}}_{V} + \underbrace{\frac{\nabla\hat{\rho}\times\nabla\bar{p}}{\bar{\rho}^2}}_{VI} + \underbrace{\frac{\nabla\bar{\rho}\times\nabla\hat{p}}{\bar{\rho}^2}}_{VII} - \underbrace{2\frac{\hat{\rho}}{\bar{\rho}^3}\left(\nabla\bar{\rho}\times\nabla\bar{p}\right)}_{VIII} + \underbrace{\nu\Delta\hat{\boldsymbol{\Omega}}}_{IX} + \underbrace{\nabla\times\hat{\boldsymbol{f}}}_{X}.$$
(8)

Again, the terms on the left hand side correspond to the material derivative of vorticity $\mathrm{D}\boldsymbol{\Omega}'/\mathrm{D}t = \partial\boldsymbol{\Omega}'/\partial t + \bar{\boldsymbol{u}}\nabla\boldsymbol{\Omega}'$, while all terms of the right hand side could be interpreted as source or sink terms of vorticity. Hence, vorticity waves are influenced or arise from

- acoustic and vortical disturbances traveling in rotational mean flow $\bar{\boldsymbol{\Omega}} = \nabla \times \bar{\boldsymbol{u}}$ such as shear and boundary layers (reaction term I and convective term II),
- stretching and bending of vorticity tubes by mean flow gradients (reaction term III),
- transformation of acoustics in strong rotational mean flow (term IV),
- strong dilatation/ compressible mean flow effects, e.g. shock-induced or amplified vorticity (term V),
- baroclinic effects due to acoustic (term VII) and entropy waves (terms VI and $VIII$),
- viscous dissipation into heat (elliptical term IX), and
- non-conservative/ rotational body forces (term X).

It is important to emphasize that the dissipation mechanisms of vorticity and entropy waves are of completely different nature: more specifically, viscosity leads to the diffusion and dissipation of vorticity waves into heat and therefore acts as a source of entropy waves. Dissipation of entropy waves is caused by heat conduction which, however, plays a minor role in comparison to the dispersion effect by flow shearing (21). In the present study the source terms for entropy and vorticity of Eq. (7) and Eq. (8), respectively, will be evaluated in a post-processing step both in order to identify and quantify the impact of different source and interaction mechanisms on the generation of indirect noise.

The linearized vorticity Eq. (8) does not quantify the energy content of the vorticity waves. Therefore an integral energy balance over the volume V with surface S and surface normal $\boldsymbol{n}$ is evaluated for the all types of fluctuations

$$\int_V \frac{\partial E}{\partial t}\mathrm{d}V + \int_S \boldsymbol{F}\cdot\boldsymbol{n}\,\mathrm{d}S = \int_V D\,\mathrm{d}V,$$
(9)

which was developed by Myers (12) and recently extended to reacting flows by Giauque et al. (22) and Brear et al. (23). In Eq. (9) the phase-averaged energy density, energy flux vector and volumetric source ($D > 0$) or

sink ($D < 0$) due to entropy and vorticity waves are represented by E, $\boldsymbol{F}$ and D, respectively (cf. Lieuwen (20))

$$E = \frac{1}{2}\mathrm{Re}\left\{\frac{\hat{p} \cdot \hat{p}^*}{2\bar{\rho}\bar{c}^2} + \frac{1}{2}\bar{\rho}\left(\hat{\boldsymbol{u}} \cdot \hat{\boldsymbol{u}}^*\right) + \hat{\rho}\left(\bar{\boldsymbol{u}} \cdot \hat{\boldsymbol{u}}^*\right) + \frac{\bar{\rho}\bar{T}\hat{s} \cdot \hat{s}^*}{2c_p}\right\}, \tag{10}$$

$$\boldsymbol{F} = \frac{1}{2}\mathrm{Re}\left\{\hat{p}\hat{\boldsymbol{u}}^* + \hat{p}\frac{\hat{\rho}^*}{\bar{\rho}}\bar{\boldsymbol{u}} + \bar{\rho}\left(\bar{\boldsymbol{u}} \cdot \hat{\boldsymbol{u}}\right)\hat{\boldsymbol{u}}^* + \left(\bar{\boldsymbol{u}} \cdot \hat{\boldsymbol{u}}\right)\hat{\rho}^*\bar{\boldsymbol{u}} + \bar{\rho}\bar{\boldsymbol{u}}\hat{T}\hat{s}^*\right\}, \tag{11}$$

$$D = \frac{1}{2}\mathrm{Re}\left\{\bar{\rho}\bar{\boldsymbol{u}} \cdot \bar{\boldsymbol{\Omega}} \times \hat{\boldsymbol{u}}^* + \hat{\rho}\hat{\boldsymbol{u}}^* \cdot \bar{\boldsymbol{\Omega}} \times \bar{\boldsymbol{u}} - \hat{s}(\bar{\rho}\hat{\boldsymbol{u}}^* + \hat{\rho}^*\bar{\boldsymbol{u}})\nabla\bar{T} + \hat{s}\bar{\rho}\bar{\boldsymbol{u}}\nabla\hat{T}^* + \left(\frac{\hat{\dot{q}}_V\hat{T}^*}{\bar{T}} - \frac{\bar{\dot{q}}_V\hat{T} \cdot \hat{T}^*}{\bar{T}^2}\right)\right\}. \tag{12}$$

In the Eqs. (10)-(12) the superscript $*$ indicates the conjugate complex amplitude. Viscous and thermal diffusion are neglected in the Eqs. (9)-(12). Note that the first term in the energy balance (9) is zero by definition under the assumption of harmonic quantities, Eq. (2). The source term is further split up into the contribution of vorticity D_v and entropy D_s, corresponding to the first two and the third and fourth term, respectively. This energy balance will supplement and confirm the source term analysis.

3.   SIMULATION MODEL

The EWG consists of a convergent-divergent nozzle with dimensions $l_{conv} = 0.13$ m, $l_{div} = 0.25$ m and throat radius of $r_{min} = 0.00375$ m. It is connected at the upstream side with a straight duct of length $l_1 = 0.25$ m and radius $r_1 = 0.015$ m. At the nozzle's downstream side a straight duct is mounted, which has a radius of $r_2 = 0.02$ m and a length of $l_2 = 1.2$ m in the the entropy excitation case and $l_2 = 0.25$ m in the scattering property determination case. Quantities with subscript 1 indicate the inlet or upstream duct, whereas the subscript 2 refers to the outlet or downstream duct. The geometry implies to solve the governing equations in cylindrical coordinates $\boldsymbol{x} = (r, \theta, z)^T$ along with the assumption of axis symmetry (i.e. $\hat{u}_\theta = 0, \partial/\partial\theta = 0$) for the variables $\hat{\rho}, \hat{\boldsymbol{u}} = (\hat{u}_r, \hat{u}_z)^T$ and $\hat{p}$. In the following two cases are regarded: The first one deals with the interaction mechanisms occurring due to the pulsed excitation of entropy waves with pulse duration $\tau = 100$ ms and temperature amplitude of $T_a = 9.4$ K. In the second case, the damping mechanisms of the acoustics are regarded which may remarkable influence the acoustic scattering properties of the nozzle. These acoustic reflection and transmission properties are important for the propagation of the indirect noise released in the turbine. They are determined by sequential upstream and downstream excitation of acoustic waves which is referred to as two source-location method (24). These two cases are based on the simulations performed by Ullrich et al. (16). The present analysis is focused on the transonic flow case under the assumption of a dry and perfect gas with constant isobaric and isochoric heat capacities.
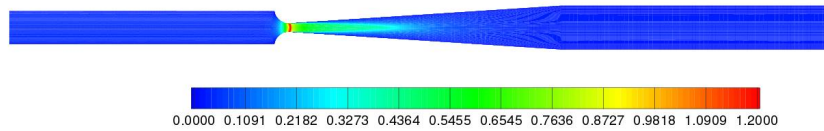

0.0000 0.1091 0.2182 0.3273 0.4364 0.5455 0.6545 0.7636 0.8727 0.9818 1.0909 1.2000

Figure 1 – Distribution of Mach number $\bar{M}$ in the mean flow through the convergent-divergent nozzle. Results by Ullrich et al. (16).

In a first step, the transonic mean flow field is calculated by stationary RANS simulations. The turbulence is described by the $k - \varepsilon$ model and the boundary layers are fully resolved up to the viscous sublayer. The convergent-divergent nozzle is discretized by a structured mesh with second order interpolation schemes. A fixed mass flow of $\dot{m} = 0.0116$ kg/s and temperature of $\bar{T}_1 = 296.15$ K are imposed at the inlet, whereas an ambient pressure of $\bar{p}_2 = 100,800$ Pa is prescribed at the outlet. The transonic mean flow field is shown in Fig. 1 where a weak shock nearby the throat is visible. The shock-boundary layer interaction leads to a small recirculation zone and further downstream to a formation of a weak jet and shear layer in the divergent nozzle part.

In the second step the LNSEs, Eqs. (3)-(5), are solved by a Galerkin/least-squares stabilized finite-element approach (FEM) as developed by Hughes et al. (25). In the case of entropy excitation the entire domain is discretized by an unstructured grid consisting of 47,946 triangular elements with second order Lagrangian shape functions, which gives a total number of 393,060 degrees of freedom. For the second case, the domain is discretized with 18,805 (154,560 degrees of freedom) triangular elements. At the inlet and outlet, acoustics are defined by an impedance boundary condition while the entering entropy wave should vanish, i.e.

$$\hat{\boldsymbol{u}} \cdot \boldsymbol{n}Z\bar{\rho}\bar{c} - \hat{p} = 0, \qquad\qquad \hat{p} - \bar{c}^2\hat{\rho} = 0. \tag{13}$$

The impedance Z is prescribed in dependence of the considered case, where
- the entropy excitation case is characterized by $Z_1 \to \infty$ (hard wall $\hat{\boldsymbol{u}} \cdot \boldsymbol{n} = 0$) and $Z_2 \in \mathbb{C}$ as measured by Bake et al. (8), and
- the acoustic scattering case is based on setting $Z_1 = Z_2 = 1$, which corresponds to non-reflecting boundaries.

In the first case, entropy excitation is realized by a volumetric energy source $\hat{q}_V$ in the linearized energy Eq. (5) which is defined in the source region located in the upstream duct. This term contains the Fourier-transformed temperature time-signal to reproduce the pulsed excitation of entropy waves. In the second case, the acoustic scattering properties are identified by subsequent excitation of acoustic waves from the upstream and downstream side by the incorporation of axial directed body force terms in the momentum Eq. (4). In the subsequent section the results are presented.

4.   RESULTS

4.1   Entropy wave excitation

In the first case, entropy waves are excited in the upstream duct of the nozzle with frequency dependent amplitude as given by the Fourier-transformed time signal. The pulsive excitation can be approximated by a short rectangular pulse whose energy content is almost completely composed by the very low frequencies. Therefore all frequency dependent variables are plotted on a logarithmic scale. The different interaction mechanisms for entropy and vorticity are evaluated spatially and visualized for a frequency of $f = 500\,\text{Hz}$ in the Figs. 2 and 3, respectively. As the entropy waves are convected downstream, they interact with the mean flow in the following way (Fig. 2(a)): Due to their acceleration acoustics are excited, which is mainly related to the absorption terms in the LNSEs. More precisely, these are terms containing mean flow gradients and fluctuating quantities such as $\hat{\boldsymbol{u}} \nabla \bar{\rho}$ and $\bar{\rho} \nabla \cdot \bar{\boldsymbol{u}}$ in the continuity Eq. (3), $\bar{\rho} \hat{\boldsymbol{u}} \nabla \bar{\boldsymbol{u}}$ and $\bar{\rho} \bar{\boldsymbol{u}} \nabla \bar{\boldsymbol{u}}$ in the momentum Eq. (4), and $\hat{\boldsymbol{u}} \nabla \bar{p}$ and $\kappa \hat{p} \nabla \cdot \bar{\boldsymbol{u}}$ in the energy Eq. (5). The acoustic waves in turn may influence the entropy waves in non-homentropic mean flow regions such as the shock and shear layer which is represented by the first coupling term in Eq. (7) and shown in Fig. 2(b). Besides, entropy waves impinging on the shock are further and directly amplified which can be seen in Figs. 2(c) and 2(d). The amplification of entropy waves by viscous dissipation occurs predominantly in the boundary layers and the shock, see Fig. 2(e). However, this effect is of minor importance, which confirms the observation that the damping dispersion effect is stronger than the amplification caused by viscous dissipation. As shown in Fig. 2(e), heat conduction is relevant in the shear layer behind the shock and in the convergent part where streamlines and therefore entropy waves are strongly stretched. In conclusion, the production of entropy waves in non-homentropic mean flow, as it typically occurs in the combustor liner cooling, dilution air injection and turbine cooling, can be source of indirect noise.

Even without any excitation of vorticity waves, they contribute to the indirect noise which is visualized in Fig. 3 and can be explained as follows: vorticity is already generated in the convergent part where mainly baroclinic effects occur in the strongly curved and stretched streamlines, cf. Figs. 3(g), 3(h) and 3(i). Temperature and density gradients, related to entropy waves, are not aligned with the mean pressure gradient because of the extreme distortion in the boundary layers. The generated vorticity waves are subsequently stretched which leads to an additional amplification as shown in Fig. 3(d). Strong dilatation effects in the mean flow further induce vorticity, either if acoustic or vorticity waves themselves impinge on the shock, see Fig. 3(e) and 3(f), respectively. Finally, the indirect sound caused by the accelerated entropy and vorticity, interacts with the shear layer of the jet behind the shock. The instability of the shear layer to acoustic disturbances is know as Kelvin-Helmholtz instability and represents by far the most important effect in the divergent nozzle, indicated by the terms *I* and *II* in Eq. (8). As shown in Fig. 3(b) and 3(c), both terms are clearly distributed over the whole shear layer which is formed due to the shock-boundary interaction. All above mentioned interaction mechanisms can represent sources of indirect noise as these vortical and temperature structures are accelerated in the following turbine blade passages in a real aero engine.

Not only the different source mechanisms can be identified, but also their order of magnitude and relevance to the overall coupling processes and the generation of indirect noise. This is done by volumetric integration of the specific source terms of the entropy and vorticity waves and shown in Fig. 4. It can be seen on the left hand side that the entropy interaction caused by irreversible mean flow effects and heat conduction is in the same order of magnitude over the whole frequency range. On the other hand the influence of viscous dissipation is remarkably lower. This stands in contrast to the vorticity interaction terms where different magnitudes are observable. Overall, the most relevant effects on vorticity production are the shear layer interactions and instabilities, the shock-induced vorticity production as well as the baroclinic effects in the convergent part.
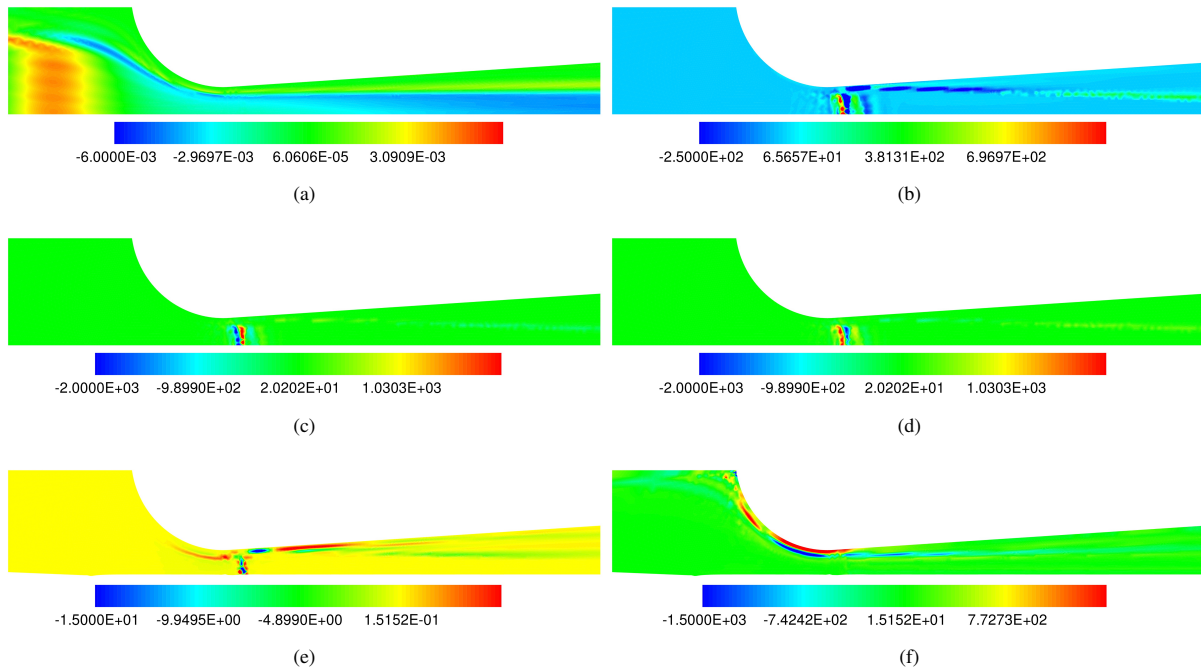
-6.0000E-03   -2.9697E-03   6.0606E-05   3.0909E-03

(a)

-2.5000E+02   6.5657E+01   3.8131E+02   6.9697E+02

(b)

-2.0000E+03   -9.8990E+02   2.0202E+01   1.0303E+03

(c)

-2.0000E+03   -9.8990E+02   2.0202E+01   1.0303E+03

(d)

-1.5000E+01   -9.9495E+00   -4.8990E+00   1.5152E-01

(e)

-1.5000E+03   -7.4242E+02   1.5152E+01   7.7273E+02

(f)

Figure 2 – Real part of the entropy wave $\hat{s}$ in $\mathrm{J/(kgK)}$ and the different entropy source and interaction terms in $\mathrm{W/m^3}$ at transonic conditions (throat Mach number $\bar{M} = 1.0$) and at a frequency of 500 Hz. 2(a): entropy wave, 2(b): term *I*, 2(c): term *II*, 2(d): term *III*, 2(e): term *IV*, and 2(f): term *V* in Eq. (7).

Finally, the integral energy balance (9) for the fluctuations is evaluated for a control volume coinciding with the convergent and divergent nozzle. As shown on the left hand side of Fig. 5, the balance

$$\int_S \boldsymbol{F} \cdot \boldsymbol{n} \mathrm{d}S - \int_V D \mathrm{d}V = 2\pi \int_0^r \boldsymbol{F} \cdot \boldsymbol{n} r \mathrm{d}r - 2\pi \int_0^l \left(\int_0^{r(z)} D r \mathrm{d}r \right) \mathrm{d}z = 0 \qquad (14)$$

is fulfilled for the low frequencies with high accuracy, whereas a deviation from zero is observed for higher frequencies. On the right hand side of Fig. 5 the different contributions from entropy and vorticity waves are plotted. Despite of the exclusive entropy wave excitation, the vortical disturbances contain more energy in the low frequency regime below 100 Hz. It is important to emphasize that the shear layer downstream of the shock is most unstable at approximately 680 Hz, which is indicated by the remarkable growth of all source terms related to vorticity. In this case maximum amplification of vorticity is caused by the disturbance of the shear layer by acoustic waves. In conclusion, these results confirm the consistence of the RANS/LNSEs approach and previous source term analysis.

4.2   Acoustic-vorticity coupling

Secondly, the interaction mechanisms between acoustic and vorticity waves are analyzed based on the work by Ullrich et al. (16) who identified the acoustic reflection and transmission properties. As shown on the left in Fig. 6, acoustic waves, which enter the domain from the upstream side and propagate towards the nozzle in downstream direction, are almost fully reflected. The upstream reflection coefficient stands at about $|R_u| \approx 0.9$ over the entire frequency range. On the other hand, the reflection of waves propagating from the downstream divergent part towards the nozzle throat, decreases notably as the frequency increases. Hence, the downstream reflection coefficient $|R_d|$ decreases from 0.95 at 200 Hz to 0.35 at 1000 Hz. This essentially different behavior is rather attributed to the loss acoustic-vorticity interaction than the entropy coupling. The volume-integrated vorticity source terms in Eq. (8) are shown in Fig. 7 for upstream (left) as well as downstream excitation (right). Obviously, the vorticity source terms are almost zero and only slightly increase with frequency for the upstream excitation. As a consequence, acoustic-vorticity interactions are weak in the convergent nozzle part, leading to an almost complete reflection of the upstream acoustic waves and the conservation of acoustic energy. As already reported in the first case, very few, if any acoustic losses occur due to baroclinic effects in regions of strongly curved streamlines. This stands in contrast to the
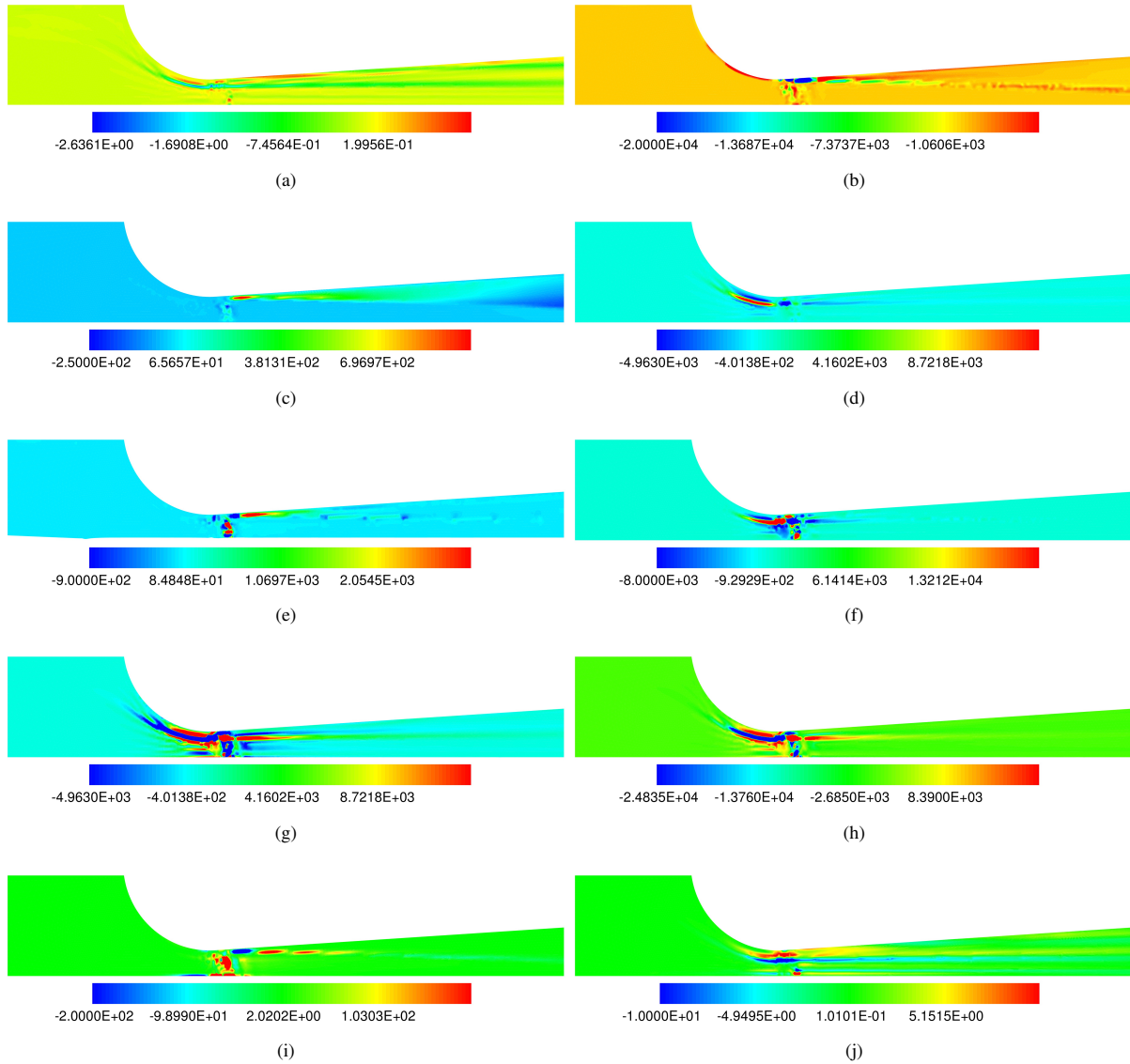
Figure 3 – Real part of the circumferential vorticity wave $\hat{\Omega}_\theta$ in $1/s$ and the different source and interaction terms in $1/s^2$ at transonic conditions (throat Mach number $\bar{M} = 1.0$) and at a frequency of $500\,\text{Hz}$. 3(a): circumferential vorticity wave, 3(b): term I, 3(c): term II, 3(d): term III, 3(e): term IV, 3(f): term V, 3(g): term VI, 3(h): term VII, 3(i): term $VIII$, and 3(j): term IX in Eq. (8).
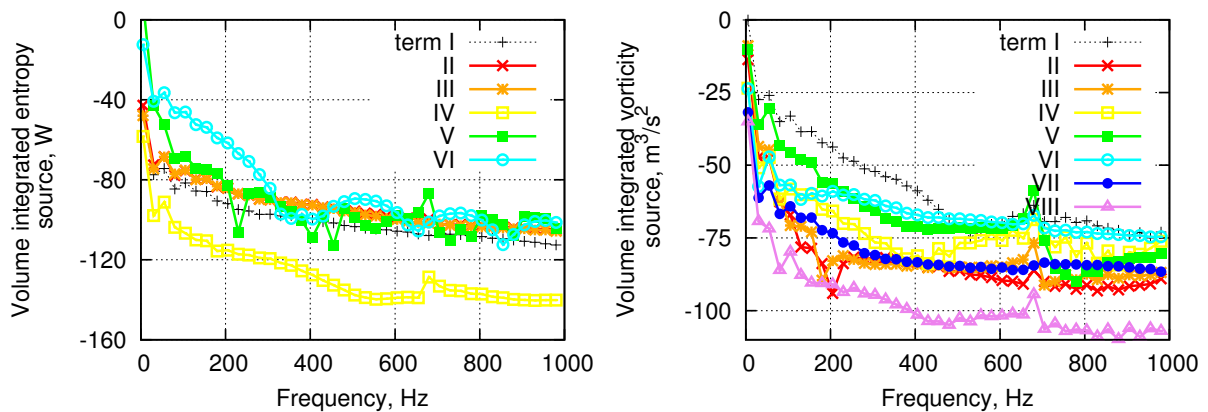

Figure 4 – Impact (absolute value) of different interaction mechanisms on the generation of entropy (left) and vorticity waves (right).
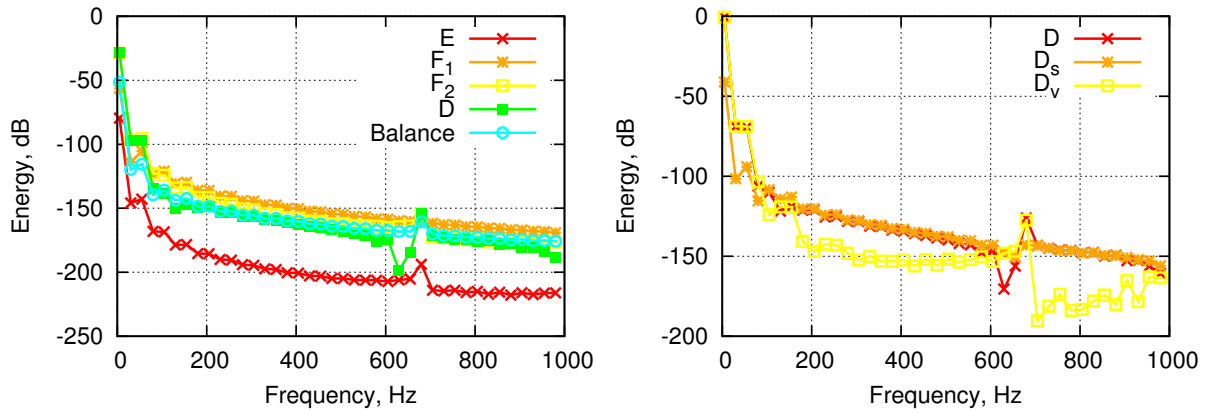
Figure 5 – Evaluation of energy equation for the entropy excitation test case where the different terms are calculated by $10\log_{10}(|E|^2)$, $10\log_{10}(|F|^2)$ and $10\log_{10}(|D|^2)$.

downstream excitation where a significant growth of the vorticity source terms with frequency is encountered. The acoustic waves are traveling from the downstream divergent part towards the nozzle throat and interact with the jet in such a manner that vorticity is generated. This represents the predominant damping effect in the divergent nozzle part (term *IV*). Besides, baroclinic effects are important while all other source mechanisms are negligible. These effects basically explain the reflection properties of the nozzle and are relevant to the propagation of indirect noise in the turbine stages.
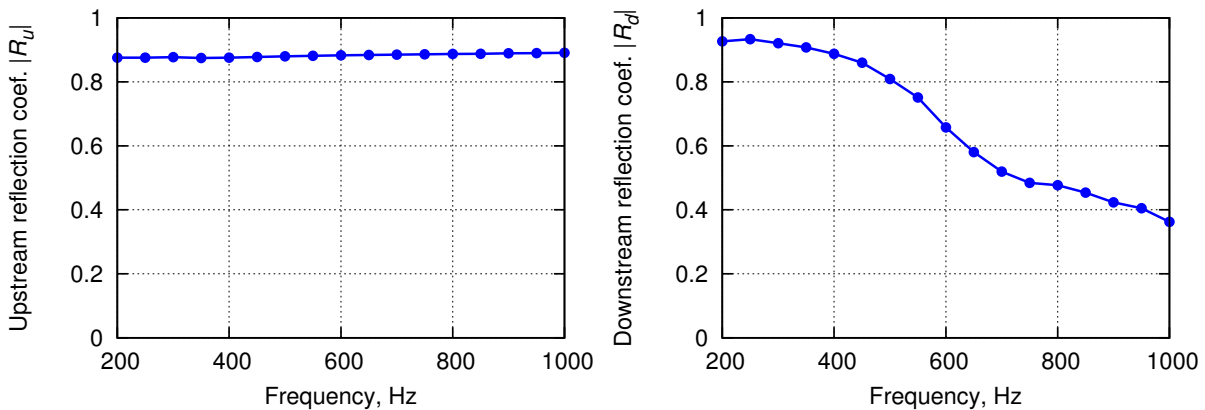

Figure 6 – Absolute value of upstream (left) and downstream (right) reflection coefficients, calculated by means of RANS/LNSEs approach on basis of the work by Ullrich et al. (16).

Furthermore, the evaluation of the disturbance energy balance Eq. (9) is consistent with the source term analysis above. The balance Eq. (14) is excellently fulfilled, except for very high frequencies above 900 Hz where slight deviations are observed. The results are plotted in Fig. 8 where the energy source term rapidly increases with frequency in the case of downstream excitation. A closer examination of the individual contribution to the total losses D shows that entropy waves D_s are of minor importance and the losses are accordingly constituted by vortical disturbances D_v for the most part. These findings are in accordance with recent studies by Schulze et al. (26).

This analysis can simply be applied to aero engine combustor liners to investigate the different kind of damping mechanisms such as vorticity shedding. The liner damping plays a crucial role for the global combustor stability. Moreover, dominant interaction frequencies between vorticity and acoustics can be determined.

5.   CONCLUSIONS

In the present paper, basic interaction mechanisms between acoustic, entropy and vorticity waves and the mean flow are identified and discussed extensively since these effects typically occur in aero engine
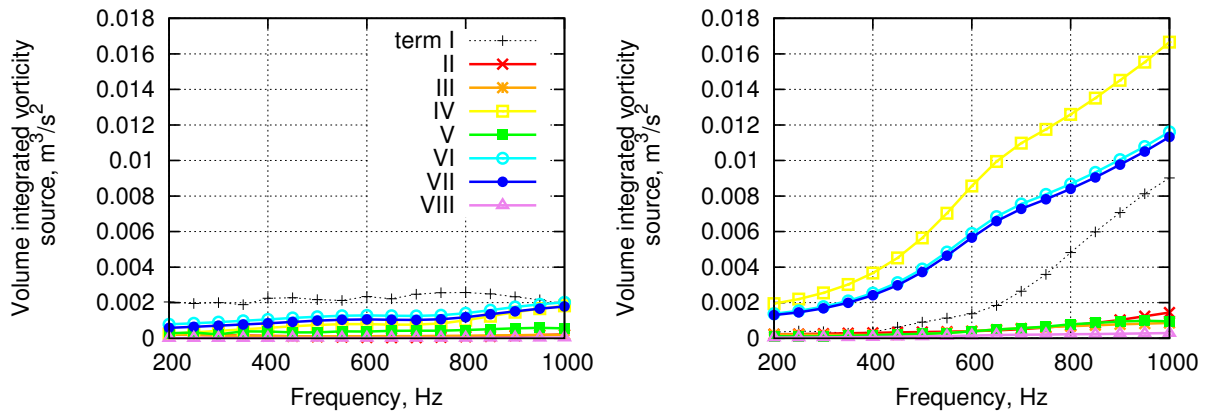
Figure 7 – Impact (absolute value) of different interaction mechanisms on the generation of vorticity with upstream (left) and downstream excitation (right).
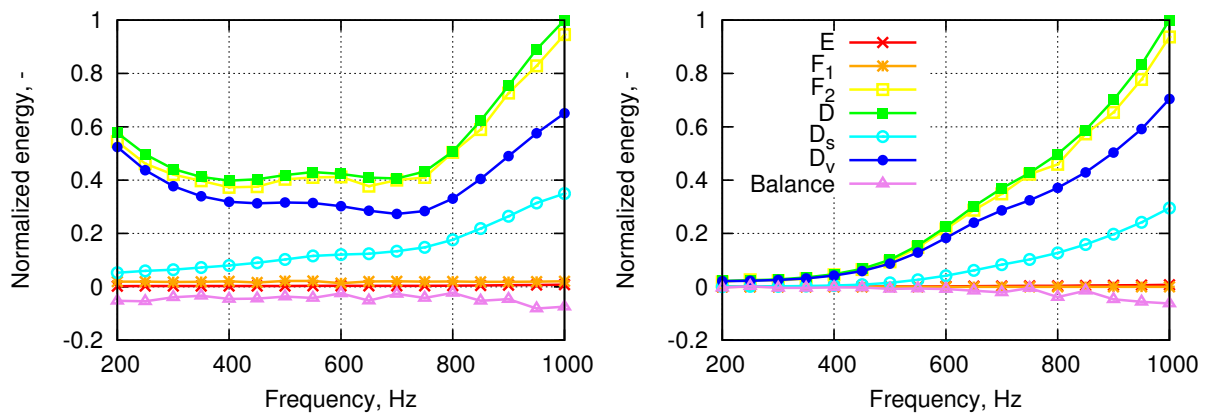

Figure 8 – Evaluation of energy equation for the scattering properties determination with upstream (left) and downstream excitation (right). The different terms are normalized by the maximum energy of $1.11 \cdot 10^{-9}$W and $2.87 \cdot 10^{-8}$W for upstream and downstream excitation, respectively.

combustors and turbines and are sources of indirect noise. Therefore a two step based hybrid RANS/LNSEs approach is applied on a convergent-divergent nozzle configuration representing the turbine vane passage flow. The source term analysis is supplemented and confirmed by an integral balance of the total disturbance energy. Furthermore, it is found that the reflection properties of the nozzle are mainly determined by the acoustic-vorticity interactions which fundamentally differ from each other in the upstream and downstream excitation case. Above all, this analysis can be applied to real aero engine configurations in order to identify and assess the impact of possible sources of indirect noise in advance during the aerothermodynamic design stage.

ACKNOWLEDGEMENTS

REFERENCES

1. Cumpsty NA, Marble FE. Core noise from gas turbine exhausts. Journal of Sound and Vibration. 1977;54(2):297–309.

2. Cumpsty NA, Marble FE. The interaction of entropy fluctuations with turbine blade rows; a mechanism of turbojet engine noise. Proceedings of the Royal Society London. 1977;357(2):323–344.

3. Leyko M, Nicoud F, Poinsot T. Comparison of direct and indirect combustion noise mechanisms in a model combustor. AIAA Journal of Propulsion and Power. 2009 Nov;47(11).

4. Duran I, Moreau S. Solution of the quasi-one-dimensional linearized Euler equations using flow invariants and the Magnus expansion. Journal of Fluid Mechanics. 2013 Apr;723:190–231.

5. Howe MS. Indirect combustion noise. Journal of Fluid Mechanics. 2010;659:267–288.

6. Kings N, Bake F. Indirect combustion noise: noise generation by accelerated vorticity in a nozzle flow. International Journal of spray and combustion dynamics. 2010;2(3):253–266.

7. Kings N, Enghardt L, Bake F. Indirect Combustion Noise: Experimental Investigation of the Vortex Sound Generation in a Chocked Convergent-divergent Nozzle. In: Proceedings of Acoustics 2012 Nantes Conference; 2012. .

8. Bake F, Richter C, Muehlbauer B, Kings N, Röhle I, Thiele F, et al. The Entropy Wave Generator (EWG): A reference case on entropy noise. Journal of Sound and Vibration. 2009;326:574–598.

9. Leyko M, Moreau S, Nicoud F, Poinsot T. Numerical and analytical modelling of entropy noise in a supersonic nozzle with a shock. Journal of Sound and Vibration. 2011;330:3944–3958.

10. Crighton DG, Dowling AP, Ffowcs Williams JE, Heckl FG M nd Leppington. Modern Methods in Analytical Acoustics: Lecture Notes. Springer-Verlag London; 1992.

11. Morfey CL. Acoustic energy in non-uniform flows. Journal of Sound and Vibration. 1971;14(2):159–170.

12. Myers MK. Transport of energy by disturbances in arbitrary steady flow. Journal of Fluid Mechanics. 1991;226:383–400.

13. Gikadi J. Prediction of Acoustic Modes in Combustors using Linearized Navier-Stokes Equations in Frequency Space. Technische Univeristät München; 2013.

14. Gikadi J, Sattelmayer T, Peschiulli A. Effects of the mean flow field on the thermo-acoustic stability of aero-engine combustion chambers; 2012. .

15. Gikadi J, Schulze M, Schwing J, Föller S, Sattelmayer T. Linearized Navier-Stokes and Euler equations for the determination of the acoustic scattering behaviour of an area extension. In: In proceedings of the 18th AIAA/CEAS Conference; 2012. .

16. Ullrich WC, Gikadi J, Jörg C, Sattelmayer T. Acoustic-entropy coupling behavior and acoustic scattering properties of a Laval nozzle. In: 20th AIAA/CEAS Aeroacoustics Conference; 2014. .

17. Schmid PJ. Dynamic mode decomposition of numerical and experimental data. Journal of Fluid Mechanics. 2010 Aug;656(2):5–28.

18. Kovásznay LSG. Turbulence in Supersonic Flow. Journal of the Aeronautical Science. 1953 Oct;20(10).

19. Chu BT, Kovásznay LSG. Non-linear interactions in a viscous heat-conducting compressible gas. Combustion and Flame. 1957;.

20. Lieuwen TC. Unsteady Combustor Physics. Cambridge University Press; 2012.

21. Sattelmayer T. Influence of the Combustor Aerodynamics on Combustion Instabilities From Equivalence Ratio Fluctuations. ASME Journal of Engineering for Gas Turbines and Power. 2003 Jan;125(11).

22. Giauque A, Poinsot T, Brear M, Nicoud F. Budget of disturbance energy in gaseous reacting flows. In: Proceedings of the Summer Program 2006; 2006. p. 285–297.

23. Brear MJ, Nicoud F, Mohsen T, Giauque A, Hawkes ER. Disturbance energy transport and sound production in gaseous combustion. Journal of Fluid Mechanics. 2012;707:53–73.

24. Munjal ML, Doige AG. Theory of a two source-location method for direct experimental evaluation of the four-pole parameters of an aeroacoustics element. Journal of Sound and Vibration. 1990;141(2):323–333.

25. Hughes TJR, Franca LP, Hulbert GM. A new finite element formulation for computational fluid dynamics: VIII. The Galerkin/least-squares method for advective-diffusive equations. Computational Methods in Applied Mechanical Engineering. 1989;73:173–189.

26. Schulze M, Wagner M, Ullrich WC, Sattelmayer T. Acoustic Damping Effects in Orifice and Perforated Plate Configurations with Sheared Flow for low Frequencies and high Mach Numbers; 2014. Submitted to Journal of Sound and Vibration.